NBAS pathogenic variants: defining the associated clinical and facial phenotype and genotype-phenotype correlations

NBAS pathogenic variants: defining the associated clinical and facial phenotype and genotype-phenotype correlations

Diana Carli[1,*], Elisa Giorgio[2,*], Francesca Pantaleoni[3], Alessandro Bruselles[4], Sabina Barresi[3], Evelise Riberi[1], Francesco Licciardi[1], Andrea Gazzin[1], Giuseppina Baldassarre[1], Simone Pizzi[3], Marcello Niceta[3], Francesca Clementina Radio[3], Cristina Molinatto[1], Davide Montin[1], Pier Luigi Calvo[5], Andrea Ciolfi[3], Nicole Fleischer[6], Giovanni Battista Ferrero[1*], Alfredo Brusco [2,7,*], Marco Tartaglia[3,*]

[1] Department of Public Health and Pediatrics, University of Torino, 10126, Torino, Italy

[2] Department of Medical Sciences, University of Torino, 10126, Torino, Italy

[3] Genetics and Rare Diseases Research Division, Ospedale Pediatrico Bambino Gesù IRCSS, 00146, Rome, Italy

[4] Department of Oncology and Molecular Medicine, Istituto Superiore di Sanità, 00161, Rome, Italy.

[5] Pediatric Gastroenterology Unit, Città della Salute e della Scienza University Hospital, 10126, Torino, Italy

[6] FDNA, Boston, MA, USA

[7] Medical Genetics Unit, Città della Salute e della Scienza University Hospital, 10126, Torino, Italy

[*] These authors equally contributed to the work.

Corresponding author:

Alfredo Brusco, Ph.D. Department of Medical Sciences, University of Torino, via Santena 19, 10126, Torino, Italy. Fax +390112365926; e-mail: alfredo.brusco@unito.it.

Short title: Genotype-phenotype correlation in NBAS disease

Conflict of interest: Nicole Fleischer is an employee of FDNA, dedicated to computer-assisted syndrome recognition technology.

Funding: this work was supported by: MURST-ex60% (to ABr) and Fondazione Bambino Gesù (Vite coraggiose, to MT). EG was supported by Fondazione Umberto Veronesi fellowship 2017-2018. This research received funding specifically appointed to Department of Medical Sciences from the Italian Ministry for Education, University and Research (Ministero dell'Istruzione, dell'Università e della Ricerca - MIUR) under the program "Dipartimenti di Eccellenza 2018–2022" project D15D18000410001, Italian Ministry of Health (Ricerca Corrente 2017 and 2018), Associazione "Enrico e Ilaria sono con noi" ONLUS, and Fondazione FORMA (to GBF).

ABSTRACT

Pathogenic variants in *NBAS* are associated with a clinical spectrum involving the hepatic, skeletal, ocular and immune systems. Here, we report on two unrelated subjects with a complex phenotype solved by whole exome sequencing, who shared a synonymous change in *NBAS* that was documented to affect transcript processing, and co-occurring with a truncating change. Starting from these two cases, we systematically assessed the clinical information available for all subjects with biallelic *NBAS* pathogenic variants (73 cases in total). We revealed a recognizable facial profile (hypotelorism, thin lips, pointed chin, and "progeroid" appearance) determined by using DeepGestalt facial recognition technology, and we provide evidence for the occurrence of genotype-phenotype correlations. Notably, severe hepatic involvement was associated with variants affecting the NBAS-Nter and Sec39 domains, while milder liver involvement and immunodeficiency were generally associated with variants located at the *N*-terminus and *C*-terminus of the protein. Remarkably, no patient was reported to carry two nonsense variants, suggesting lethality of complete *NBAS* loss-of-function.

Key words: NBAS; acute liver failure; face2gene; facial recognition technology; genotype-phenotype correlation; splicing variant.

MAIN TEXT

Three phenotypes have been associated with biallelic inactivating/hypomorphic variants in the neuroblastoma amplified sequence (NBAS; MIM# 608025): 1) infantile liver failure syndrome 2 (ILF2; MIM# 616483), an autosomal recessive condition characterized by isolated hepatic involvement with recurrent episodes of acute liver failure during intercurrent febrile illness (Haack et al., 2015); 2) short stature, optic nerve atrophy, Pelger-Huët anomaly (hyposegmented neutrophil nucleus) (SOPH; MIM# 614800) (Maksimova et al., 2010), which involves skeletal, ocular and immune system in the absence of frank hepatic involvement; 3) a severe skeletal, ocular and neurological phenotype consistent with the clinical diagnosis of acrofrontofacionasal dysostosis type 1, in the absence of both liver and immunological involvement (Palagano et al., 2018; Prontera et al., 2011).

A wide spectrum of pathogenic variants throughout the coding sequence of *NBAS* have been associated with ILF2, whereas SOPH has been linked to the recurrent homozygous c.5741G>A missense change (p.Arg1914His). This genotype has been frequently reported in an isolated Russian Yakut population due to a founder effect (Maksimova et al., 2010). In addition, acrofrontofacionasal dysostosis type 1 has been described in a single consanguineous family segregating a splice site change (c.6237-3C>G) affecting transcript processing (skipping of exon 48), and resulting in a truncated protein (Palagano et al., 2018).

Over time, ILF2 patients with more complex phenotypes have been reported, presenting with diverse involvement of hepatic, skeletal, ocular and immune systems (Balasubramanian et al., 2017; Kortum et al., 2017; Park & Lee, 2017; Staufner et al., 2016; Sunwoo, Kim, Kim, Oh, & Lee, 2018). In the majority of cases, psychomotor development and cognitive development are normal. However, in some cases, neurological involvement has been reported, varying from mild developmental delay to severe intellectual disability (Balasubramanian et al., 2017; Capo-Chichi et al., 2015; Kortum et al., 2017; Megarbane et al., 2008; Staufner et al., 2016; Sunwoo et al., 2018).

NBAS encodes a component of an endoplasmic reticulum (ER) tethering complex involved in Golgi-to-ER retrograde transport (Haack et al., 2015). NBAS interacts with SNARE proteins that are known to participate in intracellular vesicular trafficking. The specific mechanism by which defective NBAS function contributes to liver disease is, however, unknown, along with its pathophysiologic link to the observed skeletal, immune, ocular and neurological involvement. While the heterogeneous phenotypes associated with biallelic inactivating/hypomorphic *NBAS* variants are suggestive of a pleiotropic effect, genotype-phenotype correlations have not been systematically explored.

Here, we report on two unrelated cases, whose clinical features included short stature, hypogammaglobinemia, ocular involvement, and elevated liver transaminases with no episodes of acute liver failure; these patients carried two novel *NBAS* variants, one of which was a recurrent synonymous change (i.e., no predicted change at the specific codon) affecting transcript processing. We systematically reviewed the clinical and molecular features of the reported cases, defined a consensus for facial features associated with *NBAS* pathogenic variants, and explored the occurrence of genotype-phenotype correlations.

Patient 1 was a 7-year-old male born from healthy non-consanguineous parents of Italian origin; the pregnancy was uneventful. Due to a previous fetal loss and maternal constitutional thrombophilic disorder, the mother was treated with heparin during pregnancy. Fetal karyotype on amniocytes was normal (46,XY). The patient was born at 38 weeks by spontaneous delivery, with an APGAR score of 9/10. Parameters at birth included reduced length: 42 cm, -3.16 standard deviation (SD) and weight,1.87 kg, -2.86 SD. In the first months of life, the patient developed congenital bilateral glaucoma that was surgically treated by trabeculectomy. Hypogammaglobulinemia was observed at the age of 7 months during hospital admission for gastroenteritis (IgG 28 mg/dl, reference range 218–907; IgA 5 mg/dl, reference range 10–85; IgM 6 mg/dl, reference range 31–116). At 18 months, the patient started subcutaneous immunoglobulin replacement therapy (0.4 g/kg/month) due to persistent low levels of IgG. At 6 years, despite optimal IgG levels, he had developed *Listeria encephalomeningitis* with subsequent hydrocephalus that required ventriculo-peritoneal shunting.

Peripheral blood smear examination carried out after the molecular diagnosis disclosed a Pelger-Huët anomaly. He presented with persistently elevated liver AST and ALT (with ALT>AST, ALT zenit 652 U/L, nadir 76 U/L, reference range 8-40 U/L). The patient never showed signs of portal hypertension; transient hepatic elastography, as well as albumin and coagulation factors, as markers of the liver's biosynthetic capacity of the liver, were all within a normal range. At 7 years old, the patient developed iron deficiency. As part of the diagnostic work-up, a duodenal biopsy showed severe villous atrophy, which suggested coeliac disease. From his first years of life, he presented hypothyroidism (TSH: 10.3 mUI/L, reference range 0.4-4.4; fT4: 1.11 mg/dL, reference range 8.8-16.5 mUI/L) in the absence of autoantibodies. He was treated with L-thyroxine. He showed delayed growth with a proportionate short stature. At 6 years, he weighed 12.0 kg (-3.8 SD), his height was 92.3 cm (-4.6 SD), and he displayed skeletal anomalies. At 1 year, whole body X-ray disclosed short diaphyseal plates at long bones, diaphyseal radial bowing, and short metacarpophalangeal bones. Developmental milestones were slightly delayed, and he presented mild dysmorphic features (Supp. Figure 1), including closely spaced eyes, anteverted nares, smooth philtrum, narrow mouth, small hands with 5^{th} finger clinodactily, and sandal gap.

Patient 2 was a 4-year-old female born from non-consanguineous, healthy, Italian parents; the pregnancy was uneventful. Due to constitutional thrombophilic disorder, the mother was treated with heparin during pregnancy. Prenatal first trimester screening using maternal blood biochemical markers showed increased α-fetoprotein, 2.76 Multiple of Median (MoM), decreased pregnancy-associated plasma protein A (0.06 MoM), and increased human chorionic gonadotropin levels (6.74 MoM). At 16 weeks, intra-uterine growth restriction was detected. Fetal karyotype on amniocytes was normal (46,XX). The patient was born after caesarean section at 28 weeks of gestation due to maternal HELLP syndrome; her APGAR score was 5/7. Assessment at birth documented a reduced length (29.6 cm, -2.45 SD), weight (550 g, -1.93 SD), and head circumference (21.6 cm, -2.3 SD). Since birth, the patient had persistently elevated liver AST and ALT levels (with ALT>AST, ALT zenit 428 U/L, nadir 101 U/L, reference range 8-40), without signs of portal hypertension. Transient

hepatic elastography and tests of the biosynthetic capacity of the liver were normal. She also presented a sacral cleft at S1 with a tethered spinal cord. At 18 months, the patient was hospitalized for gastroenteritis and severe hypogammaglobulinemia (IgG: 93 mg/dl, normal range: 442–1139) with decreased IgA and IgM (5 and 15 mg/dl, respectively, normal ranges: 21–150 and 43–184). At 24 months, due to persistent low IgG levels, she started subcutaneous immunoglobulin replacement therapy (0.27 g/kg/month). Peripheral blood smear examination carried out after the molecular diagnosis disclosed a Pelger-Huët anomaly. At 4 years of age, she presented delayed growth with a proportionate short stature (weight 10.8 kg, height 87.8 cm; respectively -3.0 and -3.1 SD), and mild developmental delay. Facial features included a broad forehead, midface retrusion with mandibular prognathism, closely spaced eyes, upslanting palpebral fissures, simplified ears with underfolded helix and small lobes, smooth philtrum, and a narrow mouth with thin lips (Supp. Figure 1). She presented retinopathy of prematurity and severe myopia with -11.50 and -12.50 diopters in the right and left eye, respectively.

In 2016, due to their complex phenotypes, the two subjects were enrolled in the "Undiagnosed Patients Program", Ospedale Pediatrico Bambino Gesù, Rome, Italy. Informed consents for the molecular analyses were obtained from the legal tutors of the two participating subjects. The study adhered to the Declaration of Helsinki standards, and was approved by the internal Ethics Committee of the Department of Medical Sciences, University of Torino, Italy. Targeted enrichment (SureSelect Clinical Research Exome V2 kit, Agilent) and massively parallel sequencing (NextSeq 500, Illumina) were performed on genomic DNA extracted from circulating leukocytes of the affected subjects and their parents. Data analysis was performed using an *in-house* implemented pipeline, which mainly takes advantage of the Genome Analysis Toolkit (GATK V.3.7) framework, as previously reported (Flex et al., 2016; Kortum et al., 2015; Niceta et al., 2015). High-quality variants with an effect on the coding sequence or affecting splice site regions were filtered against public databases (dbSNP150 and gnomAD V.2.0) to retain i) private and clinically associated variants, ii) annotated variants with an unknown frequency or having MAF <0.1%, and occurring with a frequency <2% in an *in-house*

database including frequency data from > 1,000 population-matched whole exome sequencing (WES). The functional impact of variants was analyzed by Combined Annotation Dependent Depletion (CADD) V.1.3, Mendelian Clinically Applicable Pathogenicity (M-CAP) V.1.0 (Jagadeesh et al., 2016; Kircher et al., 2014), and using InterVar V.0.1.6 to obtain clinical interpretation according to ACMG/AMP 2015 guidelines (Li & Wang, 2017). WES statistics and findings are reported in Supp. Tables S1 and S2. Among the high-quality variants found in patient 1 (11,978) and patient 2 (14,859) predicted to have a functional impact, six genes (patient 1) and four genes (patient 2) with variants compatible with either a recessive or dominant transmission model that passed the public and in-house database filters were used for further analyses. These genes were prioritized taking into account both the predicted impact on protein function and biological relevance of the relative genes allowed to identify compound heterozygosity for two variants in *NBAS* in both subjects. Specifically, each subject carried a heterozygous truncating variant (subject 1: NM_015909.3: c.1501C>T, p.Arg501*; subject 2: NM_015909.3: c.686dupT, p.230Glnfs*4), which was found to occur in trans with a concomitant rare (1/245,982; gnomad.broadinstitute.org)(Lek et al., 2016) synonymous substitution [c.6840G>A, p.(Thr2280Thr)] affecting the last nucleotide of exon 51. Splicing site score analysis predicted disruption of the adjacent splice site donor (Supp. Table 3). Variant validation and segregation were attained by Sanger sequencing, confirming the recessive pattern of inheritance (Figure 1A-D). The synonymous variant did not occur in >1,000 population-matched exomes. Visual inspection of flanking informative markers did not allow tracking back of any ancestral relationship between the two families, suggesting either they were distantly related or the mutation arose independently. The three variants were submitted to the ClinVar database (submission SUB4766863).

To verify the predicted disruptive effect of c.6840G>A, total RNA was extracted from peripheral blood mononuclear cells obtained from the two probands and their heterozygous parents and DNAse digested (Direct-Zol RNA MiniPrep system, Zymo Research, Irvine, CA); cDNA was then obtained from 1 µg RNA (M-MLV Reverse Transcriptase kit, Applied Biosystem, Wilmington, DE, USA). The effect of the c.6840G>A substitution on transcript processing was assessed by direct

sequencing of the relevant portion of the *NBAS* cDNA (primers listed in Supp. Table S4). As shown, the variant altered *NBAS* transcript splicing leading to skipping of exon 51 and, in turn, to a mature mRNA variant encoding for a protein that lacked an in-frame portion of 43 amino acids residues within the *C*-terminal region (p.Gly2238_Thr2280del) (Figure 1E-G). Real-time RT-PCR analysis using the Universal Probe Library system (UPL; Roche diagnostics, Risch-Rotkreuz, Switzerland) showed that both probands had a reduced expression of the *NBAS* gene compared to their mothers or an healthy control, likely due to the degradation of alleles carrying the truncating variants by nonsense mediated decay (NMD). Moreover, we evaluated the relative amount of the wild-type (WT) allele versus the exon 51 skipped allele, using assays spanning the exon 51-52 junction (WT) or the exon 50-52 junction (allele with exon 51 skipping), respectively (primers listed in Supp. Table S4). As expected, the c.6840G>A substitution caused skipping of exon 51 in ~40% and in ~90% of total *NBAS* mRNA level from mothers (carriers) and probands, respectively.

Nonspecific dysmorphic features have been previously reported in patients with biallelic pathogenic *NBAS* variants (Staufner et al., 2016). To explore this issue systematically, we compared 28 frontal facial images collected from 16 patients (published and present cases; cohort including 10 females and 6 males, age range: 0.6 - 37 years, median age 9 years, ethnicity: 14 Europeans and 2 Arabs) and unaffected controls using the Face2Gene research application (version 18.1.8) (www.face2gene.com), with the facial recognition technology called DeepGestalt (FDNA Inc, Boston, USA), which has been described by (Gurovich et al., 2019). Controls included a total of 16 unrelated age- and gender-matched individuals. There was a difference in profiling between patients with biallelic *NBAS* pathogenic variants and controls. The most characteristic facial features emerging in *NBAS* patients' composite photo included hypotelorism, thin upper lip, pointed chin, and reduced subcutaneous fat conferring a "progeroid" appearance. These traits were more evident when the comparisons were performed in children vs. those observed when all cases were included (Figure 2A-F). This may explain why previous observations did not identify a recognizable facial gestalt in subjects with biallelic *NBAS* pathogenic variants.

So far, 47 different pathogenic *NBAS* variants have been reported in 71 individuals. To explore possible genotype-phenotype correlations, the available clinical data were collected (Supp. Table S5) (Balasubramanian et al., 2017; Capo-Chichi et al., 2015; Kortum et al., 2017; Maksimova et al., 2010; Megarbane et al., 2008; Regateiro et al., 2017; Segarra et al., 2015; Staufner et al., 2016)(E-P03.292008: European Society of Human Genetics 2018 meeting). A total of 36 patients have been reported to carry the homozygous p.Arg1914His change associated with the SOPH phenotype (Maksimova et al., 2010; Park & Lee, 2017), while two patients were reported to have a skeletal phenotype associated with the homozygous c.6237-3C>G splice site change (Palagano et al., 2018; Prontera et al., 2011). We evaluated the remaining 37 cases with biallelic *NBAS* variants for possible genotype-phenotype correlations. Pathogenic variants included 24 sequence changes with predicted loss-of-function (LOF) (nonsense, frameshift, out-of-frame splicing changes); 21 missense variants; three splice site changes leading to in-frame deletions, and two changes predicting single amino acid deletions. Of note, genotypes could be divided into two major categories. A first group (8 cases) was characterized by the combination of two missense variants or a missense and an in-frame deletion (Figure 2G, top), while a second group (27 cases) was characterized by compound heterozygosity for a LOF variant and a missense or in-frame splicing/deletion (Figure 2G, bottom). The phenotype associated with biallelic *NBAS* pathogenic variants mainly affects the liver, with immunodeficiency, skeletal defects, and ophthalmologic and neurologic anomalies also representing recurrent features. Of note, all patients from group 1 were found to present with acute liver failure (ALF) in the absence of immunodeficiency as a concomitant associated feature. Based on this observation, and assuming an equivalent inactivating effect for each of the reported nonsense and frameshift variants, independently from the type of change and its location, we explored any possible correlation between phenotype and position of the second pathogenic variant. Remarkably, a relationship between liver involvement and variant position was observed since all patients who experienced ALF episodes were found to carry pathogenic variant(s) between exon 7 and exon 40, the majority causing amino acid changes within the NBAS-Nterm and Sec39 functional domains. The only two patients in which both

elevated liver transaminases (ELT) and acute liver failure (ALF) had been formally ruled out were the two sisters affected by acrofrontofacionasal dysostosis type 1 caused by the homozygous c.6237-3C>G change, resulting in the production of an aberrant protein (Palagano et al., 2018; Prontera et al., 2011). The 34 SOPH patients, homozygotes for the c.5741G>A missense change (p.Arg1914His), had not been investigated for hepatic involvement. However, two siblings with the same genotype presented with skeletal, ocular, possible immunological involvement (frequent infections had not been investigated) and mild hepatic involvement with persistent ELT without episodes of ALF (Park & Lee, 2017). This suggests that patients with SOPH may have a subclinical hepatic involvement that should be investigated. Among the reported *NBAS* genotypes, skipping of exon21/c.1042C>T (p.Pro348Ser) has been described in two siblings (Staufner et al., 2016) presenting with severe hepatic involvement with ALF, and differing only in the short stature of one. Of note, immunodeficiency is the only other clinical feature that seems to strictly correlate with the location of pathogenic variants, with a pattern reverse to liver failure: cases with immunodeficiency have missense variants at the *N*-terminal or *C*-terminal regions of the protein. The p.Glu447Lys and p.Cys426Trp variants in exon 14, just downstream of the NBAS-Nter domain, were the only exceptions, and were both associated with a combined ALF and immunodeficiency. Despite the occurrence of correlations, we however noted the presence of a discordant neurodevelopmental phenotype in two unrelated patients with the same genotype (p.Glu943*/p.Leu903Arg) presenting with ALF, short stature and without immunological or ocular involvement. One presented mild intellectual disability (ID) and epilepsy, the other presented severe ID. It remains to be established whether this is a feature of variable expressivity associated with p.Leu903Arg, or if it is due to the different genetic backgrounds, or if it is a complication of severe ALF-related hepatic encephalopathy (Staufner et al., 2016). In this context, in addition to immunologic, ocular and skeletal features being commonly reported in patients with biallelic *NBAS* pathogenic variants, shared features of the two affected subjects in this study included bilateral glaucoma, hypothyroidism and a celiac disease in patient 1, and a sacral cleft with tethered spinal cord in patient 2. Re-analysis of WES data did not identify variants in genes that could be

related to these phenotypes, suggesting a possible contribution of defective NBAS function, and an expansion of NBAS-related phenotypes.

A notable finding of this study is the identification of a recurrent pathogenic synonymous variant demonstrated to affect proper *NBAS* transcript processing and resulting in skipping of an exon encoding part of the *C*-terminal tail. A different variant causing skipping of a different exon coding for an adjacent portion of the protein has previously been reported (Figure 2G), further documenting the functional relevance of this still structurally uncharacterized region of the protein. It is now well-established that synonymous variants may alter gene expression through modulation of splicing, mRNA stability, and translation, and disturbing these processes may contribute to human disease (Mueller, Larsen, Garibaldi, Hatfield, & Hertel, 2015; Supek, Minana, Valcarcel, Gabaldon, & Lehner, 2014). This finding further highlights the current need to optimize the bioinformatics workflow required to attain an accurate functional annotation of the large number of variants that are routinely identified by genome-wide sequencing, as well as the importance of not underestimating synonymous variations when screening for disease-causing variants (Gelfman et al., 2017; Livingstone et al., 2017; Pantaleoni et al., 2017).

In conclusion, we report two unrelated subjects with a trait associated with defective NBAS function sharing a previously unreported pathogenic "synonymous" change demonstrated to affect proper *NBAS* transcript processing. Assessing the clinical features and signs of affected subjects with biallelic *NBAS* variants documents the occurrence of a recognizable facial profile for these patients, and provide the first evidence for the occurrence of clinically relevant genotype-phenotype correlations in diseases associated with *NBAS* pathogenic variants.

ACKNOWLEDGEMENTS

Authors are indebted with the families for taking part into this study.

REFERENCES

Balasubramanian, M., Hurst, J., Brown, S., Bishop, N. J., Arundel, P., DeVile, C., . . . Skerry, T. M. (2017). Compound heterozygous variants in NBAS as a cause of atypical osteogenesis imperfecta. *Bone, 94*, 65-74. Retrieved from https://www.ncbi.nlm.nih.gov/pubmed/27789416. doi:10.1016/j.bone.2016.10.023

Capo-Chichi, J. M., Mehawej, C., Delague, V., Caillaud, C., Khneisser, I., Hamdan, F. F., . . . Megarbane, A. (2015). Neuroblastoma Amplified Sequence (NBAS) mutation in recurrent acute liver failure: Confirmatory report in a sibship with very early onset, osteoporosis and developmental delay. *Eur J Med Genet, 58*(12), 637-641. Retrieved from https://www.ncbi.nlm.nih.gov/pubmed/26578240. doi:10.1016/j.ejmg.2015.11.005

Flex, E., Niceta, M., Cecchetti, S., Thiffault, I., Au, M. G., Capuano, A., . . . Tartaglia, M. (2016). Biallelic Mutations in TBCD, Encoding the Tubulin Folding Cofactor D, Perturb Microtubule Dynamics and Cause Early-Onset Encephalopathy. *Am J Hum Genet, 99*(4), 962-973. Retrieved from https://www.ncbi.nlm.nih.gov/pubmed/27666370. doi:10.1016/j.ajhg.2016.08.003

Gelfman, S., Wang, Q., McSweeney, K. M., Ren, Z., La Carpia, F., Halvorsen, M., . . . Goldstein, D. B. (2017). Annotating pathogenic non-coding variants in genic regions. *Nat Commun, 8*(1), 236. Retrieved from https://www.ncbi.nlm.nih.gov/pubmed/28794409. doi:10.1038/s41467-017-00141-2

Gurovich, Y., Hanani, Y., Bar, O., Nadav, G., Fleischer, N., Gelbman, D., . . . Gripp, K. W. (2019). Identifying facial phenotypes of genetic disorders using deep learning. *Nat Med, 25*(1), 60-64. Retrieved from https://www.ncbi.nlm.nih.gov/pubmed/30617323. doi:10.1038/s41591-018-0279-0

Haack, T. B., Staufner, C., Kopke, M. G., Straub, B. K., Kolker, S., Thiel, C., . . . Prokisch, H. (2015). Biallelic Mutations in NBAS Cause Recurrent Acute Liver Failure with Onset in Infancy. *Am J Hum Genet, 97*(1), 163-169. Retrieved from https://www.ncbi.nlm.nih.gov/pubmed/26073778. doi:10.1016/j.ajhg.2015.05.009

Jagadeesh, K. A., Wenger, A. M., Berger, M. J., Guturu, H., Stenson, P. D., Cooper, D. N., . . . Bejerano, G. (2016). M-CAP eliminates a majority of variants of uncertain significance in clinical exomes at high sensitivity. *Nat Genet, 48*(12), 1581-1586. Retrieved from https://www.ncbi.nlm.nih.gov/pubmed/27776117. doi:10.1038/ng.3703

Kircher, M., Witten, D. M., Jain, P., O'Roak, B. J., Cooper, G. M., & Shendure, J. (2014). A general framework for estimating the relative pathogenicity of human genetic variants. *Nat Genet, 46*(3), 310-315. Retrieved from http://www.ncbi.nlm.nih.gov/pubmed/24487276. doi:10.1038/ng.2892

Kortum, F., Caputo, V., Bauer, C. K., Stella, L., Ciolfi, A., Alawi, M., . . . Kutsche, K. (2015). Mutations in KCNH1 and ATP6V1B2 cause Zimmermann-Laband syndrome. *Nat Genet, 47*(6), 661-667. Retrieved from http://www.ncbi.nlm.nih.gov/pubmed/25915598. doi:10.1038/ng.3282

Kortum, F., Marquardt, I., Alawi, M., Korenke, G. C., Spranger, S., Meinecke, P., & Kutsche, K. (2017). Acute Liver Failure Meets SOPH Syndrome: A Case Report on an Intermediate Phenotype.

Pediatrics, 139(1). Retrieved from https://www.ncbi.nlm.nih.gov/pubmed/28031453. doi:10.1542/peds.2016-0550

Lek, M., Karczewski, K. J., Minikel, E. V., Samocha, K. E., Banks, E., Fennell, T., . . . Exome Aggregation, C. (2016). Analysis of protein-coding genetic variation in 60,706 humans. *Nature, 536*(7616), 285-291. Retrieved from http://www.ncbi.nlm.nih.gov/pubmed/27535533. doi:10.1038/nature19057

Li, Q., & Wang, K. (2017). InterVar: Clinical Interpretation of Genetic Variants by the 2015 ACMG-AMP Guidelines. *Am J Hum Genet, 100*(2), 267-280. Retrieved from https://www.ncbi.nlm.nih.gov/pubmed/28132688. doi:10.1016/j.ajhg.2017.01.004

Livingstone, M., Folkman, L., Yang, Y., Zhang, P., Mort, M., Cooper, D. N., . . . Zhou, Y. (2017). Investigating DNA-, RNA-, and protein-based features as a means to discriminate pathogenic synonymous variants. *Hum Mutat, 38*(10), 1336-1347. Retrieved from https://www.ncbi.nlm.nih.gov/pubmed/28649752. doi:10.1002/humu.23283

Maksimova, N., Hara, K., Nikolaeva, I., Chun-Feng, T., Usui, T., Takagi, M., . . . Onodera, O. (2010). Neuroblastoma amplified sequence gene is associated with a novel short stature syndrome characterised by optic nerve atrophy and Pelger-Huet anomaly. *J Med Genet, 47*(8), 538-548. Retrieved from https://www.ncbi.nlm.nih.gov/pubmed/20577004. doi:10.1136/jmg.2009.074815

Megarbane, A., Samaras, L., Chedid, R., Chouery, E., Chretien, D., Caillaud, C., . . . Jalkh, N. (2008). Developmental delay, dysmorphic features, neonatal spontaneous fractures, wrinkled skin, and hepatic failure: a new metabolic syndrome? *Am J Med Genet A, 146A*(24), 3198-3201. Retrieved from https://www.ncbi.nlm.nih.gov/pubmed/19012336. doi:10.1002/ajmg.a.32579

Mueller, W. F., Larsen, L. S., Garibaldi, A., Hatfield, G. W., & Hertel, K. J. (2015). The Silent Sway of Splicing by Synonymous Substitutions. *J Biol Chem, 290*(46), 27700-27711. Retrieved from https://www.ncbi.nlm.nih.gov/pubmed/26424794. doi:10.1074/jbc.M115.684035

Niceta, M., Stellacci, E., Gripp, K. W., Zampino, G., Kousi, M., Anselmi, M., . . . Tartaglia, M. (2015). Mutations Impairing GSK3-Mediated MAF Phosphorylation Cause Cataract, Deafness, Intellectual Disability, Seizures, and a Down Syndrome-like Facies. *Am J Hum Genet, 96*(5), 816-825. Retrieved from http://www.ncbi.nlm.nih.gov/pubmed/25865493. doi:10.1016/j.ajhg.2015.03.001

Palagano, E., Zuccarini, G., Prontera, P., Borgatti, R., Stangoni, G., Elisei, S., . . . Sobacchi, C. (2018). Mutations in the Neuroblastoma Amplified Sequence gene in a family affected by Acrofrontofacionasal Dysostosis type 1. *Bone, 114*, 125-136. Retrieved from https://www.ncbi.nlm.nih.gov/pubmed/29929043. doi:10.1016/j.bone.2018.06.013

Pantaleoni, F., Lev, D., Cirstea, I. C., Motta, M., Lepri, F. R., Bottero, L., . . . Tartaglia, M. (2017). Aberrant HRAS transcript processing underlies a distinctive phenotype within the RASopathy clinical spectrum. *Hum Mutat, 38*(7), 798-804. Retrieved from https://www.ncbi.nlm.nih.gov/pubmed/28390077. doi:10.1002/humu.23224

Park, J. W., & Lee, S. J. (2017). Foveal hypoplasia in short stature with optic atrophy and Pelger-Huet anomaly syndrome with neuroblastoma-amplified sequence (NBAS) gene mutation. *J AAPOS*. Retrieved from https://www.ncbi.nlm.nih.gov/pubmed/28115293. doi:10.1016/j.jaapos.2016.09.030

Prontera, P., Urciuoli, R., Siliquini, S., Macone, S., Stangoni, G., Donti, E., . . . Belcastro, V. (2011). Acrofrontofacionasal dysostosis 1 in two sisters of Indian origin. *Am J Med Genet A, 155A*(12), 3125-3127. Retrieved from https://www.ncbi.nlm.nih.gov/pubmed/22052670. doi:10.1002/ajmg.a.34295

Regateiro, F. S., Belkaya, S., Neves, N., Ferreira, S., Silvestre, P., Lemos, S., . . . Diogo, L. (2017). Recurrent elevated liver transaminases and acute liver failure in two siblings with novel bi-allelic mutations of NBAS. *Eur J Med Genet, 60*(8), 426-432. Retrieved from https://www.ncbi.nlm.nih.gov/pubmed/28576691. doi:10.1016/j.ejmg.2017.05.005

Segarra, N. G., Ballhausen, D., Crawford, H., Perreau, M., Campos-Xavier, B., van Spaendonck-Zwarts, K., . . . Bonafe, L. (2015). NBAS mutations cause a multisystem disorder involving bone, connective tissue, liver, immune system, and retina. *Am J Med Genet A, 167A*(12), 2902-2912. Retrieved from https://www.ncbi.nlm.nih.gov/pubmed/26286438. doi:10.1002/ajmg.a.37338

Staufner, C., Haack, T. B., Kopke, M. G., Straub, B. K., Kolker, S., Thiel, C., . . . Hoffmann, G. F. (2016). Recurrent acute liver failure due to NBAS deficiency: phenotypic spectrum, disease mechanisms, and therapeutic concepts. *J Inherit Metab Dis, 39*(1), 3-16. Retrieved from https://www.ncbi.nlm.nih.gov/pubmed/26541327. doi:10.1007/s10545-015-9896-7

Sunwoo, Y., Kim, Y. M., Kim, E. N., Oh, S. H., & Lee, B. H. (2018). Severe form of neuroblastoma amplified sequence deficiency in an infant with recurrent acute liver failure. *Pediatr Int, 60*(3), 302-304. Retrieved from https://www.ncbi.nlm.nih.gov/pubmed/29575310. doi:10.1111/ped.13476

Supek, F., Minana, B., Valcarcel, J., Gabaldon, T., & Lehner, B. (2014). Synonymous mutations frequently act as driver mutations in human cancers. *Cell, 156*(6), 1324-1335. Retrieved from https://www.ncbi.nlm.nih.gov/pubmed/24630730. doi:10.1016/j.cell.2014.01.051

LEGEND TO FIGURES

Figure 1. Pedigrees and molecular data.

Panels A and B: pedigrees of the two probands and variant segregation analysis. Sanger sequence electropherograms are reported in panels C and D. Panel E: a schematic representation of exon 50-52 genomic region of the *NBAS* gene. The c.6840G>A variant affects the last base of exon 51, and it is predicted to alter the intron 51 donor splice site (intronic splicing consensus sites are shown). Arrows above the exons indicate the primers used for exon 51 skipping analysis. Panel F: gel electrophoresis analysis of the cDNA between exons 50 and 52. Skipping of exon 51 is also present in control subjects, but it is clearly enhanced in subjects carrying the pathogenic variant. The two bands were gel-purified and Sanger sequenced. Panel G: electropherograms show the wild-type exon 50-51 junction (above) and the aberrant exon 50-52 junction (below). CTRLs: healthy controls. Panel H: total *NBAS* mRNA levels (left) and relative amounts of WT vs. exon 51 skipped isoforms (right), analyzed by RT-PCR. Both probands showed a reduced expression of total *NBAS*, compatible with NMD, associated with the nonsense variants inherited from the fathers. In the mothers, carriers of the c.6840G>A variant, approximately 40% of *NBAS* transcript lacks exon 51. In probands, this transcript is over 90% of the total *NBAS*. A small amount of exon 51 skipping is also present in controls.

Figure 2. NBAS-associated facial phenotype and genotype-phenotype correlations.

Panels A-D: composite photos obtained from patients (Balasubramanian et al., 2017; Capo-Chichi et al., 2015; Kortum et al., 2017; Maksimova et al., 2010; Megarbane et al., 2008; Regateiro et al., 2017; Staufner et al., 2016) and age/gender matched controls. Facial features of subjects with biallelic inactivating/hypomorphic *NBAS* variants include hypotelorism, thin upper lip, pointed chin, and a progeroid appearance. These traits are more evident in children (panels B and D) than in the group that includes all cases (panels A and C). The software used loaded images to generate a score distribution reported for all cases (panel E above) and children (panel E below). Statistical

evaluation was performed measuring the Area Under the Curve (AUC) of the Receiver Operating Characteristic (ROC) curve and calculating P value (p=0.003 for all, and p=0.008 for children, panel F).

Panel G: distribution of the known disease-causing *NBAS* pathogenic variants. Cartoon showing the 52 coding exons of the *NBAS* gene (reference sequence NM_015909). The two known protein domains NBAS-Nter (aminoacids 90-371) and Sec39 (aminoacids 726-1365) are also represented. We reported only missense/in-frame deletions/splicing variants leading to an in-frame deletion. Top: pathogenic variants found in homozygous or compound heterozygous state. Bottom: pathogenic variants reported in compound heterozygosity concomitantly with a nonsense variant. Variant p.Arg1914His is associated with SOPH when in homozygosis (in blue). The c.6237-3C>G change (skipping of exon 48) is associated with a specific skeletal phenotype when occurring in homozygosity (in green)(Palagano et al., 2018; Prontera et al., 2011). Variants in yellow are associated with acute liver failure and are mostly missense in the functional domains. Variants in pink are associated with immunodeficiency and are located at the edges of the protein. Only two variants, p.Glu447Lys and p.Cys426Trp, are both associated with liver involvement and immunodeficiency.

Supp. Fig. 1. Patients' facial dysmorphisms and limb features.

Panel A and B show full body and face pictures of the studied affected subject (II-2) from family 1. Note closely spaced eyes, anteverted nares, smooth philtrum, and narrow mouth. Panels C and D display the small hands with clinodactily of the fifth finger, and the sandal gap, respectively. In panels E and F, facial features of patient II-2 from family 2 are reported. She had broad forehead, midface retrusion with mandibular prognathism, closely spaced eyes with upslanting palpebral fissures, simplified ears with underfolded helix and small lobe, smooth philtrum, narrow mouth with thin lips.

Supplementary Table S1. Whole exome sequencing data output of patient 1.

	Patient 1
Target regions coverage, 2x[1]	96.7%
Target regions coverage, 20x[1]	85.9%
Average sequencing depth on target[1]	89x
Number of variants with predicted functional effect	11,978
Novel, clinically associated, and unknown/low frequency variants[2]	552
Putative disease genes (Autosomal Recessive/X-linked inheritance)[3]	6[4]
Putative candidate gene (Autosomal Recessive/X-linked inheritance)	1, *NBAS*
Genes with putative *de novo* variants[3]	0
Putative candidate genes (Autosomal Dominant inheritance)	0

[1]Referred to SureSelect Clinical Research Exome V2 (Agilent).

[2]MAF <0.1% in gnomAD V. 2.0 databases, and frequency <2% in our *in-house* database.

[3]Filtering retained functionally relevant variants by excluding variants predicted as benign by CADD and M-CAP algorithms or benign/likely benign by interVar.

[4]*GPR143* (c.1045G>A, p.Glu349Lys), *MED12* (c.5400+6C>T), *LRCH2* (c.998+4A>G), *NBAS* (c.6840G>A, p.Thr2280Thr; c.1501C>T, p.Arg501*), *PCLO* (c.7168C>A, p.Pro2390Thr; c.1094_1123dupCTCTTGGTCCTGCTAAGCCTCCAGCTCAGC, p.Pro365_Gln374dup), *SYK* (c.-50C>T, c.1182-7C>G).

Supplementary Table S2. Whole exome sequencing data output of patient 2.

	Patient 2
Target regions coverage, 2x[1]	96.5%
Target regions coverage, 20x[1]	86.0%
Average sequencing depth on target[1]	84x
Number of variants with predicted functional effect	14,859
Novel, clinically associated, and unknown/low frequency variants[2]	389
Putative disease genes (Autosomal Recessive)[3]	4[4]
Putative candidate gene (Autosomal Recessive)	1, *NBAS*
Genes with putative *de novo* variants[3]	4[5]
Putative candidate genes (Autosomal Dominant inheritance)	0

[1]Referred to SureSelect Clinical Research Exome V2 (Agilent).

[2]MAF <0.1% in gnomAD V. 2.0 databases, and frequency <2% in our *in-house* database.

[3]Filtering retained functionally relevant variants by excluding variants predicted as benign by CADD and M-CAP algorithms or benign/likely benign by interVar.

[4]*ABCA12* (c.1475A>G, p.Asn492Ser; c.-46G>T, premature start codon gain), *CRYBG3* (c.3352_3372delATTGGGACAGAAGTAACCCCA, p.Ile1118_Pro1124del; c.5719A>G, p.Thr1907Ala), *GARS* (c.-343G>T; c.1945G>A, p.Asp649Asn), *NBAS* (c.6840G>A, p.Thr2280Thr; c.686dupT, p.Ser230fs).

[5]*TUBE1* (c.-48A>T), *ATM* (c.1202A>G, p.Gln401Arg), *MYH14* (c.6088_6089insGCC, p.Ser2030delinsCysPro), *ZNF534* (c.1742_1822delATAGGAATATTCATACTGGAGAGAAGCCTCACAGTTGTAATGAATGTGGCAAGGTCTTCAGTCGGAATTCACACCTTGCGC, p.His581_Ala607del).

Supplementary Table S3. Donor splice site score change at c.6840G>A variant obtained by Alamut visual software (Alamut Visual v.2.10.0 on 2/6/2018).

Donor Sites

	SSF [0-100]	MaxEnt [0-12]	NNSPLICE [0-1]	GeneSplicer [0-24]	HSF [0-100]
Threshold	*≥ 70*	*≥ 0*	*≥ 0.4*	*≥ 0*	*≥ 65*
Exon 51 – c.6831					= 65.87
Exon 51 – c.6840 N	74.83 ⇒ —	8.56 ⇒ 3.04 *(-64.5%)*	0.99 ⇒ —	7.84 ⇒ 2.42 *(-69.1%)*	83.32 ⇒ 72.74 *(-12.7%)*
Intron 51 – c.6840+92					= 76.30

Natural Splice Site

Supplementary Table S4. List of primers used.

Analysis of cDNA: PCR amplification and Sanger sequencing of exon 51 skipped allele

Primer	Sequence
cNBAS-50F	5'- ACGATGGAGAACAAGGAAGG
cNBAS-52R	5'- GGAGTGGAGACACACTTCACC

Analysis of NBAS mRNA levels

Assay	Exon-exon junction	Primer	UPL Roche #	sequence
total NBAS levels	Exon 12-exon13	cNBAS-12F	71	5'- tgaagcaacaaggggaatg
		cNBAS-13R		5'- cctccaatcaggattaaggtca
wt allele	Exon 51-exon52	cNBAS-51F	68	5'- gcaaatcacggcagtcacta
		cNBAS-52R		5'- agggagtggagacacacttca
exon 51 skipping	Exon 50-exon52	cNBAS-50F	68	5'- ttgaaaatgtgtcgctctttgt
		cNBAS-52R		5'- agggagtggagacacacttca

Supplementary Table S5. Genotypes and phenotypes of NBAS reported cases (update 23 August 2018).

Mutations				Clinical features				
Allele 1	**Exon/ Intron**	**Allele2**	**Exon/ intron**	**Hepatic**	**Immuno**	**Ocular**	**Skeletal**	**N**
c.850A>T; p.Lys284*	10	c.284C>T; p.Ala95Val	4	ELT, hepatomegaly	PHA, hypogammaglobulinemia, reduced natural killer cells, no response to vaccinations	Optic atrophy, retinal dystrophy	Short stature, skeletal dysplasia, reduced bone density	psych dev in
c.409C>T; p.Arg137Trp	7	c.409C>T; p.Arg137Trp	7	ALF, hepatosplenomegaly	no PHA	no	Large fontanels with delayed closure, neonatal spontaneous fractures, reduced bone density, delayed bone age. NO short stature	Axia dev
c.686dupT; p.230Qfs*4	9	c.558_560del; p.Ile187del	8	ALF	no PHA	Optic atrophy	Short stature	psych dev in
c.1749G>A; p.Trp583*	17	c.680A>C; p.His227Pro	9	ALF, hepatomegaly	Urticaria and angioedema, low numbers of CD8+ T cells and high CD4+/CD8+ T cell-ratios, high IgE. PHA not assesed.	no	Short stature, delayed bone age, reduced bone density	ps de
c.2926del; p.Ser976Profs*16	25	c.809G > C; p.Gly270Ala	10	ALF	PHA not assesed	no	NO short stature	ps dev in

c.2203-3C>G; skipping exon 21	IVS 20	c.1042C>T; p.Pro348Ser	12	ALF	PHA not assesed	no	NO short stature	ps dev in
c.2203-3C>G; skipping exon 21	IVS 20	c.1042C>T; p.Pro348Ser	12	ALF	PHA, erythema nodosum, Crohn's disease	no	short stature	
c.409C>T; p.Arg137Trp	7	c.1186T>A; p.Trp396Arg	14	ALF, hepatomegaly	PHA, reduced natural killer cells	NO optic atrophy, myopia, astigmatism	Short stature, skeletal dysplasia, fractures	dev d su in
c.5454_5455delTT; p.Leu1818fs*16	44	c.1339G>A; p.Glu447Lys	14	ALF	hypogammaglobulinemia, no PHA	Pale disc, vascular attenuation and narrowing, and occlusive appearance in the fundus of both eyes	Large anterior fontanelle, short stature, skeletal dysplasia, reduced bone density, fractures	mark dev delay callos v
deletion exons 49-50; p.Val1528Glyfs*2	49	c.1278T>G; p.Cys426Trp	14	ALF	PHA, hypogammaglobulinemia	no	Short stature	psych dev in
c.1187G>A; p.Trp396*	14	c.2330C>A; p.Pro777His	21	ALF	PHA not assesed	no	NO short stature	psych dev in
c.5389+1G>T; skipping exon 43	IVS 44	c.2407G>A; p.Glu803Lys	22	ALF, hepatosplenomegaly	PHA not assesed	no	NO short stature	ps de
c.118-2A>G; skipping exon 2	IVS 1	c.2524G>T; p.Val842Phe	23	ALF	PHA not assesed	no	Short stature	ps de
c.2708T>; p.Leu903Arg	24	c.2708T>G; p.Leu903Arg	24	ALF	no PHA	no	Short stature	Epile c bord
c.2827G>T; p.Glu943*	25	c.2708T>G; p.Leu903Arg	24	ALF	no PHA	no	Short stature	In disal mild
c.2819A>C; p. His940Pro	25	c.2819A>C; p. His940Pro	25	ALF, hepatomegaly	PHA not assesed	Not assesed	Poor growth	ps de

c.1533_1545del; p.Ile 512Thrfs*4	15	c.2951T>G; p.Ile984Ser	26	ALF	PHA not assesed	no	Short stature	dev d su in
c.603_605delCCT; p.Leu202del	8	c.3164T>C; p.Leu1055Pro	28	ALF	no PHA, Celiac disease	no	Short stature	psych dev in
c.686dupT; p.230Qfs*4	9	c.3164T>C; p.Leu1055Pro	28	ALF	PHA not assesed	no	Short stature	psych dev in
c.3010C>T; p.Arg1004*	26	c.3164T>C; p.Leu1055Pro	28	ALF	no PHA	no	NO short stature	psych dev in
c.173-2A>G; skipping exon 3	IVS 2	c.3363A>G; p.Ile1121Met	30	ALF	PHA not assesed	No	NO short stature	psych dev in
c.209+1G>A; skipping exon 3	IVS 3	c.3596G>A; p.Cys1199Tyr	31	ALF	PHA not assesed	Not assesed	Unreported	
c.6611_6612insCA; p.M2204Ifs*3	50	c.3596G>A; p.Cys1199Tyr	31	ALF	PHA not assesed	Not assesed	Unreported	psy de
c.586C>T; p.Gln196*	8	c.3596G>A; p.Cys1199Tyr	31	ALF	PHA not assesed	Not assesed	Unreported	psy de
c.3928A>G; p.Thr1310Ala	33	c.4228 A>G; p.Thr1410Ala	36	ALF	PHA not assesed	Not assesed	Unreported	U
c.2827G>T; p.Glu943*	25	deletion exons 39-40; p.Val2145_Glu2237del	39-40	ALF	PHA, hypogammaglobulinemia, lymphopenia during crisis	Optic atrophy	Short stature, skeletal dysplasia	Mild dela neu
c.2032C>T; p.Gln678*	19	c.5741G>A; p.Arg1914His	45	ELT	PHA, hypogammaglobulinaemia	Optic atrophy, nystagmus	Large anterior fontanelle, short stature, reduced bone density, fractures,	Mild

							pamidronate therapy	
c.2827G>T; p.Glu943*	25	c.5741G>A; p.Arg1914His	45	ELT	PHA, hypogammaglobulinemia, neutropenia, no response to vaccinations, reduced B cells	Optic atrophy, progressive visual loss, strabismus	Large anterior fontanelle, short stature, skeletal dysplasia, delayed bone age, multiple Wormian bones	H dev delay in
c.3010C>T; p.Arg1004*	26	c.5741G>A; p.Arg1914His	45	ELT	PHA, hypogammaglobulinaemia, progressive lymphopenia	Optic atrophy, nystagmus and myopia	Large anterior fontanelle, short stature, skeletal dysplasia, reduced bone density, fractures, multiple Wormian bones	M in disal
c.5741G>A; p.Arg1914His	45	c.5741G>A; p.Arg1914His	45	ELT	PHA	Decreased visual acuity, optic atrophy, foveal hypoplasia, achromatopsia, nystagmus, thickness of the retinal nerve fiber layer	Short stature	in
c.5741G>A; p.Arg1914His	45	c.5741G>A; p.Arg1914His	45	ELT not assesed	PHA	Optic atrophy, strabismus, myopia	Short stature, delayed bone age	in
c.6237-3C>G; skipping exon 48	48	c.6237-3C>G; skipping exon 48	48	no ELT	PHA not assesed	Optic atrophy, severe visual deficit, exotropia	Large fontanelles, skeletal dysplasia	hypo neuro d abn ep corp sever
c.686dupT; p.230Qfs*4	9	c.6840G>A; p.Thr2280Thr	51	ELT	PHA, hypogammaglobulinemia, coeliac disease	Congenital glaucoma	Short stature, skeletal dysplasia,	Dev delay in

							reduced bone density	
c.1501C>T; p.Arg501*	15	c.6840G>A; p.Thr2280Thr	51	ELT	PHA, hypogammaglobulinemia	Retinopathy of prematurity, severe myopia	Short stature	Dev delay in

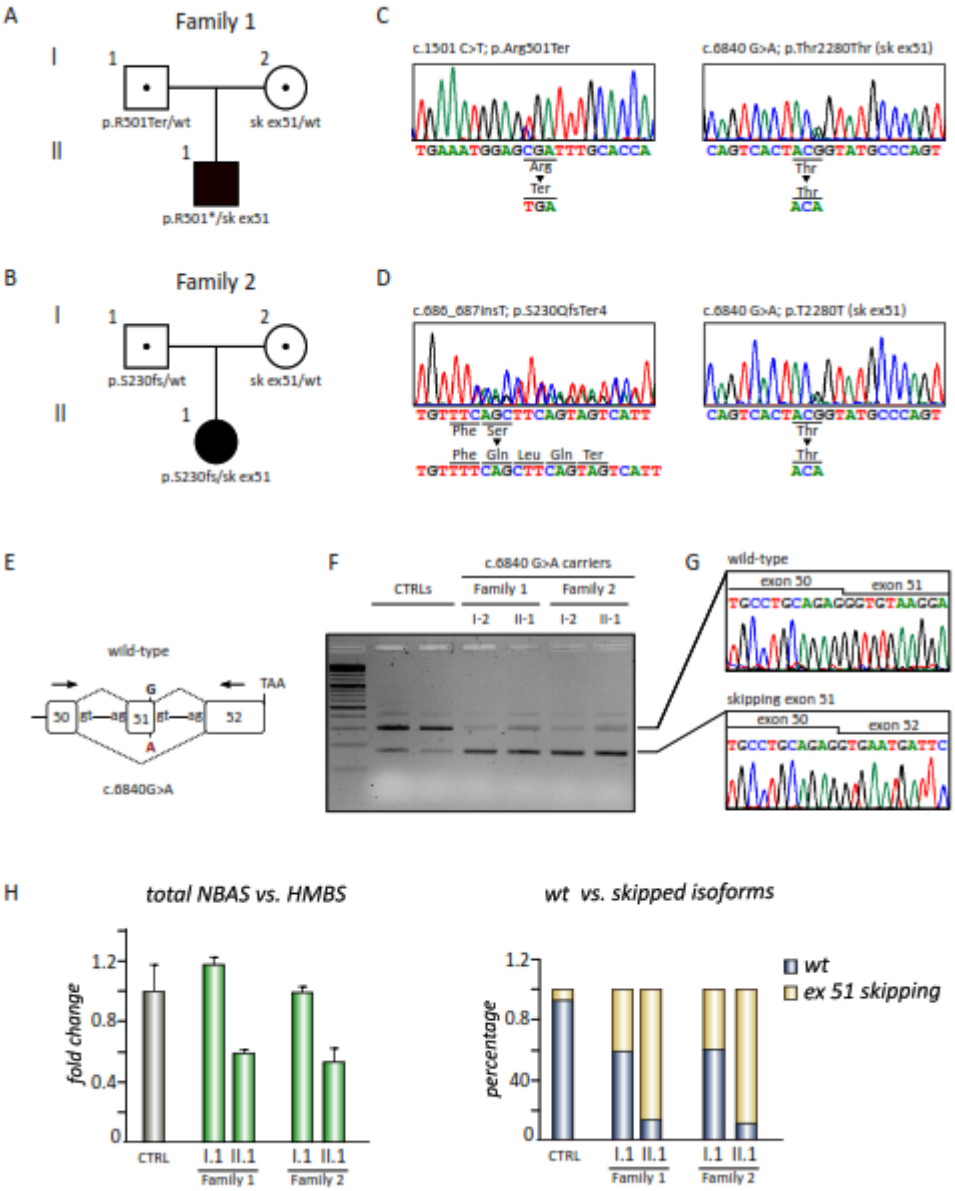
A
Family 1
I
1
2
p.R501Ter/wt
sk ex51/wt
II
1
p.R501*/sk ex51
B
Family 2
I
1
2
p.S230fs/wt
sk ex51/wt
II
1
p.S230fs/sk ex51
C
c.1501 C>T; p.Arg501Ter
TGAAATGGAGCGATTTGCACCA
Arg
Ter
TGA
c.6840 G>A; p.Thr2280Thr (sk ex51)
CAGTCACTACGGTATGCCCAGT
Thr
Thr
ACA
D
c.686_687InsT; p.S230QfsTer4
TGTTTCAGCTTCAGTAGTCATT
Phe Ser
Phe Gln Leu Gln Ter
TGTTTCAGCTTCAGTAGTCATT
c.6840 G>A; p.T2280T (sk ex51)
CAGTCACTACGGTATGCCCAGT
Thr
Thr
ACA
E
wild-type
G
TAA
50
51
52
A
c.6840G>A
F
c.6840 G>A carriers
CTRLs
Family 1
Family 2
I-2
II-1
I-2
II-1
G
wild-type
exon 50
exon 51
TGCCTGCAGAGGGTGTAAGGA
skipping exon 51
exon 50
exon 52
TGCCTGCAGAGGTGAATGATTC
H
total NBAS vs. HMBS
fold change
1.2
0.8
0.4
0
CTRL
I.1
II.1
Family 1
I.1
II.1
Family 2
wt vs. skipped isoforms
percentage
1.2
0.8
40
0
wt
ex 51 skipping
CTRL
I.1
II.1
Family 1
I.1
II.1
Family 2

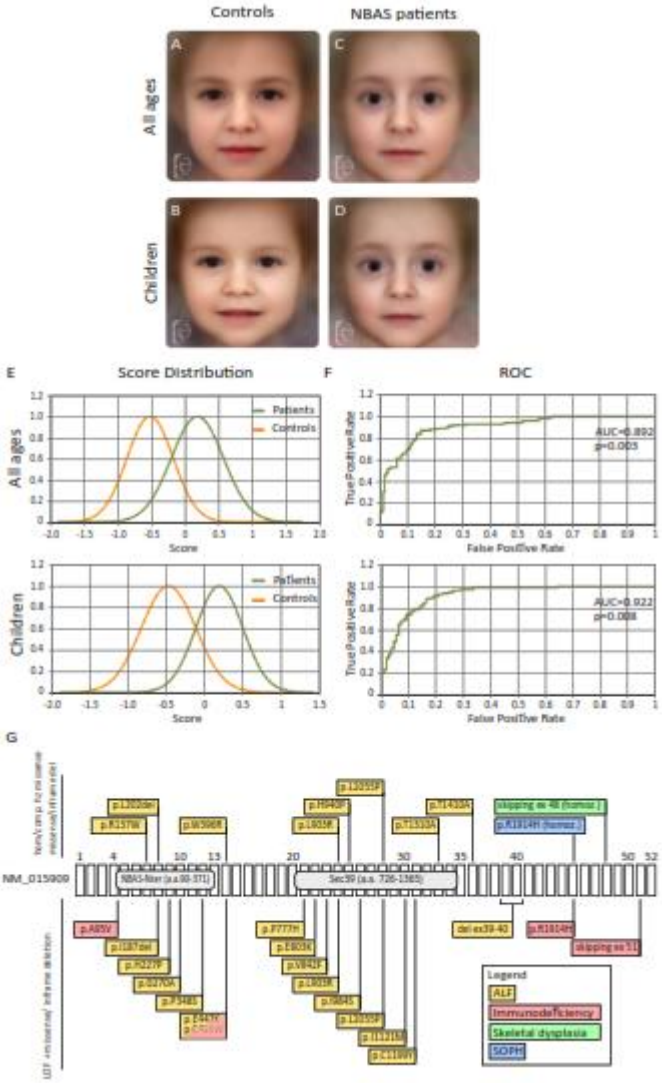
Controls
NBAS patients
A
C
All ages
B
D
Children
E
Score Distribution
F
ROC
All ages
Patients
Controls
Score
True Positive Rate
False Positive Rate
AUC=0.892
p=0.005
Children
AUC=0.922
p=0.008
G
NM_015909
NBAS-like (a.a.00-371)
Sec39 (a.a. 726-1365)
Legend
ALF
Immunodeficiency
Skeletal dysplasia
SOPH